ADVANCED FUNCTIONAL MATERIALS
www.afm-journal.de



# Highly Concentrated and Conductive Reduced Graphene Oxide Nanosheets by Monovalent Cation–$\pi$ Interaction: Toward Printed Electronics

*Seung Yol Jeong, Sung Hun Kim, Joong Tark Han, Hee Jin Jeong, Soo Yeon Jeong, and Geon-Woong Lee**

**A novel route to preparing highly concentrated and conductive reduced graphene oxide (RGO) in various solvents by monovalent cation–$\pi$ interaction. Previously, the hydrophobic properties of high-quality RGO containing few defects and oxygen moieties have precluded the formation of stable dispersion in various solvents. Cation–$\pi$ interaction between monovalent cations, such as $Na^+$ or $K^+$, and six-membered $sp^2$ carbons on graphene were achieved by simple aging process of graphene oxide (GO) nanosheets dispersed in alkali solvent. The noncovalent binding forces introduced by the cation–$\pi$ interactions were evident from the chemical shift of the $sp^2$ peak in the solid $^{13}C$ NMR spectra. Raman spectra and the *I-V* characteristics demonstrated the interactions in terms of the presence of *n*-type doping effect due to the adsorption of cations with high electron mobility (39 $cm^2$/Vs). The RGO film prepared without a post-annealing process displayed superior electrical conductivity of 97,500 S/m at a thickness of 1.7 μm. Moreover, mass production of GO paste with a concentration as high as 20 g/L was achieved by accelerating the cation–$\pi$ interactions with densification process. This strategy can facilitate the development of large scalable production methods for preparing printed electronics made from high-quality RGO nanosheets.**

## 1. Introduction

Graphene has received much interest due to its superior mechanical and electrical properties, including a high Young's modulus, high specific surface area, high electrical conductivity, and high carrier mobility.[1–4] Single-layer graphene is a promising candidate for the production of electronic devices, composites, and energy storage applications. Several methods for producing single-layer graphene, including mechanical cleavage, epitaxial growth, chemical vapor deposition (CVD), and chemically modified graphene (CMG), have been described.[5–8] The CVD and CMG methods provide the most practical approaches for adaptation to large-scale manufacturing processes. Here, we focused on the use of CMG for solution-based electronics printing and the mass production of high concentrated and conductive single-layer graphene. The production of CMG involves several essential steps for the chemical exfoliation and subsequent reduction of graphite oxide.[9] Colloidal suspensions of high-quality CMG, which contain few oxygen functional groups and defects, have been unobtainable due to the hydrophobic nature of graphene. The synthesis of graphite oxide was described by Brodie in 1859 as a starting material for graphene.[10] The synthetic methods typically used today are those of Brodie, Saudenmaier, Hummers, and Offman and involve extensive oxidation by a strong acid to increase the interlayer distance in the graphite. Hummers' method is the most common, and is the fastest and most effective way to form an aqueous dispersion with a large interlayer distance typical of highly oxidized graphite oxide.[11] Compared to the Hummers method, Brodie's method yields lower contamination and higher quality graphite oxide, although the interlayer distance is small.[12,13] To improve the exfoliation of graphite oxide prepared by Brodie's method and the dispersion GO, the pH should be controlled by addition of NaOH or KOH. We used a modified Brodie method accordingly to produce high-quality RGO. However, reduction of GO to RGO tends to result in agglomeration in aqueous solutions due to hydrophobic interactions among the RGO sheets.[14] A stable dispersion of RGO is particularly important for preserving the unique properties of the nanostructures. Surfactants, such as polymers, have been introduced to reduce agglomeration;[15] however, the presence of polymers in RGO can alter the characteristics of RGO that are most desirable for applications. Using a modified Hummers method, Li et al. prepared an aqueous dispersion of RGO without a polymeric surfactant by controlling the pH using ammonium ions and dialysis.[16] Park et al. reported the preparation of a colloidal suspension containing hydrazine-reduced potassium-modified RGO by addition of aqueous KOH. These studies suggested that the introduction

Dr. S. Y. Jeong, S. H. Kim, Dr. J. T. Han, Dr. H. J. Jeong, S. Y. Jeong, Dr. G.-W. Lee
Graphene Hybrid World Class Laboratory
Nano Carbon Materials Research Group
Korea Electrotechnology Research Institute (KERI)
Changwon, 641-120, Korea
E-mail: gwleephd@keri.re.kr

DOI: 10.1002/adfm.201200242

of potassium ions could stabilize the RGO suspensions by binding to the negatively charged carboxylate groups at the edge sites in the graphene sheets.[17] The RGO suspension has not been achieved in various organic solvents. Moreover, the electrical conductivity was not enhanced compared to the recent works.[18] In 1996, the unusual cation–$\pi$ interactions on benzene and other aromatic systems have been introduced by Dougherty et al., who investigated their physical origin in the presence of the cations $Li^+$, $Na^+$, and $K^+$.[19] Noncovalent binding forces can be induced between a monopole (cation) and a quadrupole (aromatic $\pi$ system). However, the stabilized RGO dispersion by monovalent cation–$\pi$ interactions has not been considered previously. The cations binding to oxygen functional groups may be weaker in less oxidized GO containing a higher fraction of six-membered $sp^2$ carbons. The cation-decorated high-quality GO can be dispersed in various solvents due to Coulombic repulsion among the cations associated with the graphene. Therefore, we hypothesized that these interactions could be used to disperse high-quality RGO containing fewer defects and oxygen functional groups.

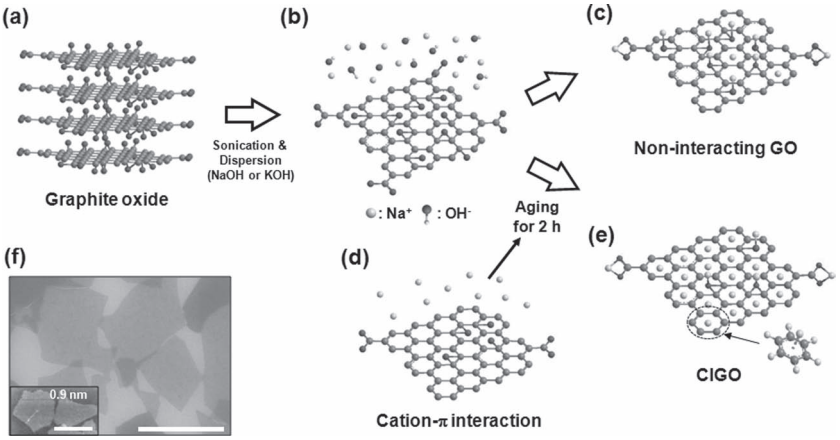


**Figure 1.** Comparison of the cation–$\pi$ interactions and the non-interacting GO. (a–c) Schematic diagrams describing the non-interacting GO. a) Morphology of graphite oxide with various oxygen functional groups. b) GO sheets dispersed in NaOH solution. c) Highly interacting cations with oxygen functional groups. (a, b, d, e) Procedure for obtaining cation–$\pi$ interacting GO. d) The intermediate state produced by mild deoxygenation by an alkaline solvent, such as NaOH, and an aging time of 2 h. e) Monovalent cations with a highly interacting aromatic $\pi$ system, compare to (c). f) FE-SEM image of CIGO on a silicon wafer (inset: AFM images of CIGO sheets). The scale bars in (f) and that in the inset indicate 2 μm.

In this work, we introduce the preparation of highly concentrated and conductive RGO, made possible by the presence of monovalent cation–$\pi$ interactions in the NaOH aqueous solution. The stability of this RGO dispersion was more sensitive to the strength of the cation–$\pi$ interactions than to the cation–oxygen functional group interactions. The longer aging times of an aqueous GO solution with addition of an alkaline solvent enhanced the dispersion stability without producing RGO aggregation after hydrazine reduction, regardless of the solvent types. The chemical shift of $^{13}C$ solid state nuclear magnetic resonance (SSNMR) and I-V characteristics verified electrostatic interactions between the $sp^2$ carbon atoms and the cations. Subsequent hydrazine reduction resulted in the uniform dispersion of RGO in a variety of solvents. Moreover, a homogeneous GO dispersion could be obtained with a concentration as high as 20 g/L without an addition of polymeric binder. The controlled stability of high-quality RGO dispersion and superior electrical conductivity of 97,500 S/m open up several possibilities for applying solution-processable RGO in the mass production of printed electronics via spray-printing, screen printing, and roll-to-roll processes.

## 2. Results and Discussion

A schematic diagram in **Figure 1** shows our strategy to stabilize the RGO dispersion by monovalent cation–$\pi$ interactions. The interactions between alkali metal ions and $sp^2$ carbons on the GO sheets do not form immediately after sonication since the cations preferably interact with carboxylic acid and hydroxyl groups on highly oxidized GO (as described in Figure 1a,b, and c). Therefore, mild reduction process of GO sheets and an aging process without mechanical perturbation are necessary to permit the monovalent cation–$\pi$ interactions (Figure 1a, b, d, and e route). To increase the six-membered sp2 carbons and stabilize the interactions with cations, we imposed an interaction time of 2 h after sonication, described here as an aging process, Figure 1d. In an aqueous solvent, the electrostatic binding enthalpy of monovalent cations to a $\pi$ system ($-\Delta H$ = 19.2 kcal/mol) was higher than that with water ($-\Delta H$ = 17.9 kcal/mol).[20] Longer aging times yielded the cation–$\pi$ interacting GO (CIGO), as shown in Figure 1e. The dispersibilities of the non-interacting GO and CIGO were similar in aqueous solutions due to the presence of oxygen functional groups in each sample. However, the significant differences between the GO and CIGO were revealed after hydrazine reduction, which desorbed the oxygen functional groups from graphene, as illustrated in **Figure 2**. These results demonstrated that the cations did not desorb from the $\pi$ system on the CIGO after deoxygenation of graphene, which weakened the interactions between the cations and the oxygen functional groups. After hydrazine reduction, the CIGO formed a dispersion of cation–$\pi$ interacting RGO (CIRGO), whereas the non-interacting GO agglomerated in solution, as shown in Figure 2c. The single-layered CIGO was uniformly distributed with a size of 2 μm and a thickness of 0.9 nm in the AFM image shown in Figure 1f.

The dispersion stabilities of the RGO solutions significantly depend on the presence of monovalent cation–$\pi$ interactions, as shown in Figure 2. The UV-vis absorbance spectra were used to monitor the RGO stability as a function of aging time of the aqueous GO solutions (1)–(3), which were permitted to incubate at room temperature without agitation after sonication for 1 h, as shown in Figure 2a. Hydrazine reduction of CIGO over 16 h at 100 °C rendered a homogeneous CIRGO dispersion in solution after an aging time of 2 h for (3), whereas the RGO aggregated and precipitated in solution due to hydrophobic interactions for the samples not permitted to age, as in (1). A

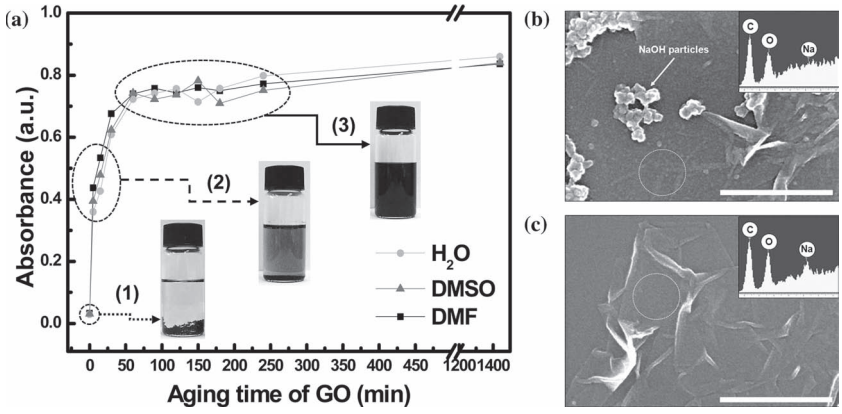


**Figure 2.** Dispersion stability of CIRGO and the non-interacting RGO. a) Absorbance spectra as a function of aging time for a GO solution in DI water, DMSO, or DMF. b) FE-SEM images of non-interacting RGO, as shown in Fig. a1 (dotted black arrow), the white arrow indicates the precipitated NaOH particles. c) Morphology of the CIRGO without residual particles, Fig. a3 (black arrow). The insets of (b) and (c) reveal the EDS results gathered at the positions indicated by white dotted circles. (The scale bars in (b) and (c) indicate 10 μm.)

longer aging time of 30 min enhanced the dispersion stability of an intermediate RGO solution state, compare (2) with (1). However, RGO sediment was observed because the degree of cation–$\pi$ interactions was not sufficient to stabilize the RGO dispersion in solution. The dispersibilities of RGO in DI water, DMSO, and DMF were similar. DMSO has been described previously as being less stabilizing toward RGO dispersions.[21] The dispersion stability of RGO as a function of GO aging time after sonication for 1 h was sensitive to the presence of monovalent cation–$\pi$ interactions. Figures 2b and 2c show the RGO sheets on silicon substrate using the solution (1) and (3) in Figure 2a. Recrystallized NaOH particles formed on the RGO surfaces in Figure 2b, whereas the CIRGO revealed clean surfaces due to the homogeneous distribution of monovalent sodium ions on the basal plane in Figure 2c. The EDS results confirmed that the relative percentage of sodium on the CIRGO surface was higher than the precipitated RGO, as shown in the insets of Figure 2b and 2c. These results demonstrated that the aging process was a crucial factor to preserve the noncovalent intermolecular monovalent cation–$\pi$ interactions in solution.

The monovalent cation–$\pi$ interactions induced a change in the chemical shifts of the graphitic carbon atoms ($sp^2$) due to electrostatic interactions with sodium ions. High-resolution $^{13}C$ SSNMR using magic angle spinning (MAS) provided signal assignments and specific structural information for the non-interacting GO and the CIGO (**Figure 3**a). The $^{13}C$ NMR spectra for GO sheets revealed three main peaks at 59.2 (epoxide: C-O-C), 69.8 (hydroxyl: C-OH), and 129.1 (graphitic carbon: $sp^2$) ppm, as reported previously.[22] A broad $CH_2$ peak was observed at 30.8 ppm. Unlike previous reports of GO, the main $sp^2$ peak was split to give signals at 132.7 and 129.1 ppm, as shown in the inset of Figure 3a. The existence of an upfield chemical shift peak (132.7 ppm) for the $sp^2$ carbons reveals the presence of interactions with $Na^+$ ions.[23] The cation–$\pi$ interaction is

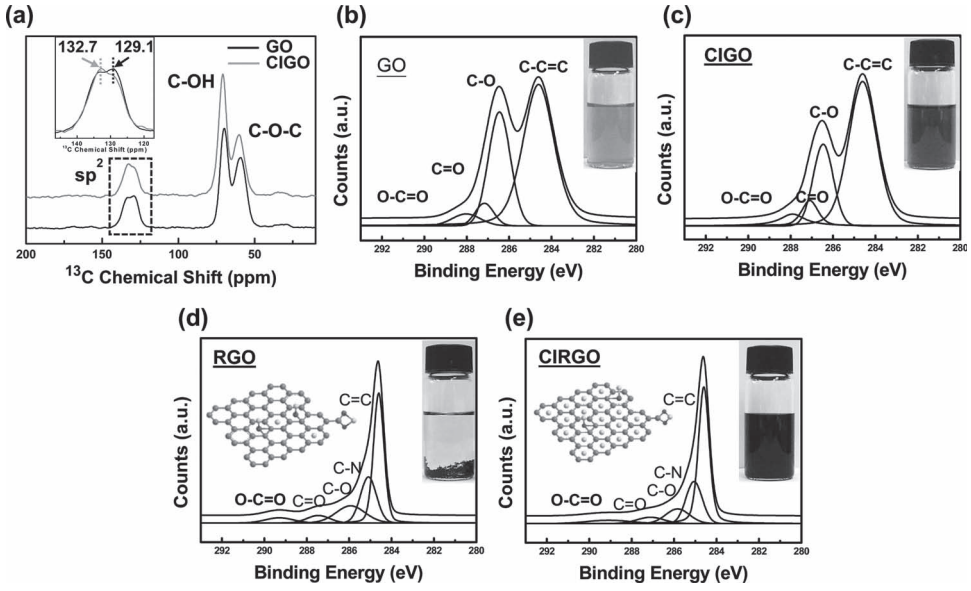


**Figure 3.** Evidence of monovalent cation–$\pi$ interactions by $^{13}C$ NMR and XPS analysis. a) $^{13}C$ NMR analysis of the non-interacting GO and CIGO, (inset: the split $sp^2$ peaks at 132.7 and 129.1 ppm). (b–e) XPS analysis of the samples. b) GO after sonication of graphite oxide for 1 hr (inset: dark yellow-colored aqueous GO solution). c) CIGO with an aging time of 1 hr (inset: dark brown CIGO solution), the hydroxyl and epoxy groups are dramatically reduced compared to those in (b). d), e) After hydrazine reduction at 100 °C for 16 h. d) Non-interacting RGO without an aging process (inset: agglomerated RGO solution and fewer interacting cations on the GO, as shown in the schematic diagrams). e) Formation of CIRGO from CIGO with a highly interacting cation and aromatic $\pi$ system (inset: black-colored CIRGO solution and cations interacting highly with the $\pi$ system, as shown in the schematic diagrams).

similar to a Coulombic interaction. It can be induced between a monopole (cation) and a quadrupole(aromatic pi system). The magnitude of this interaction was described by binding enthalpies of $Na^+$ and $K^+$ ions which shows 28 and 19 kcal/mol respectively.[19] These smaller ions can be tightly bound with aromatic $\pi$ system. As a result, these are increased Coulombic energy. Significantly, the chemical shift can be described by Coulomb potential.[24] The potential may contribute the spin-orbital interaction on the cation–$\pi$ system. In addition, this shift was induced by ring current effects, which influenced by attached cations on the aromatic rings.[25] In case of any cation inside the aromatic ring, the shielding field induced on the $\pi$ system because the applied magnetic field had the opposite direction. Therefore, the upfield shift occured at the 132.7 ppm. In the CIGO, the chemical shift of the $sp^2$ peak was 132.7 ppm, with a higher peak intensity compared to that for non-interacting GO. These results demonstrated the presence of monovalent cation–$\pi$ interactions between the $sp^2$ and sodium ions in the CIGO. In the case of non-interacting GO, the sodium ions may have been adsorbed even onto the basal plane due to the addition of sodium chlorate as an intercalant during acid treatment. However, the relative intensity of the GO was lower than that of the CIGO at 132.7 ppm. Significantly, the CIRGO formed a stable dispersion, in contrast with the non-interacting RGO, as shown in Figure 2. X-ray photoemission spectroscopy (XPS) was used to determine the atomic percentage of oxygen functional groups, including C-O (hydroxyl and epoxy, ~287.6 eV), C = O (Carbonyl, ~288.3 eV), O-C = O (carboxy, ~290.1 eV), and C = C/C-C ($sp^2$ and $sp^3$, ~284.6 eV) on the unreacted GO, CIGO, RGO, and CIRGO, as shown in Figure 3b–3e and Table S2.[26] The relative intensities of the hydroxyl and epoxy groups on the basal plane of the CIGO were reduced after mild reduction with a hydroxide solution as reported previously.[27] The aqueous GO was yellow in color due to a large number of oxygen functional groups, as shown in Figure 3b. In the GO, the color of the solution changed to dark brown upon mild reduction, as shown in Figure 3c. The atomic ratio of C/O of CIGO (4.17) exceeded that for GO (1.96), as listed in **Table 1**. The CIGO was significantly reduced at the basal planes and adsorbed cations onto the $\pi$ system during aging process. Subsequent hydrazine reduction at 100 °C for 16 h deoxygenated the functional groups of GO to yield a black solution, as shown in Figure 3d and 3e. Despite similar atomic percentages for the samples (Table 1), the non-interacting RGO agglomerated in solution due to hydrophobic surface interactions. These results suggested that the electrostatic adsorption of cations to the aromatic $\pi$ system was not affected by hydrazine reduction.

**Table 1.** Analysis of the atomic weight percentages and atomic ratios of C/O for the GO, CIGO, RGO, and CIRGO samples.

| Sample | C [wt%] | O [wt%] | C/O |
|---|---|---|---|
| GO | 59.56 | 40.44 | 1.96 |
| CIGO | 75.81 | 24.19 | 4.17 |
| RGO | 83.34 | 16.66 | 6.66 |
| CIRGO | 83.74 | 16.26 | 6.86 |

The presence of residual cations on the basal plane significantly affected the dispersion stability of RGO. Moreover, mild reduction by a hydroxide solution was a crucial factor for enhancing monovalent cation–$\pi$ interactions. We attempted to introduce the interactions by adding NaCl to the aqueous solution. However, the RGO coagulated in solution, most likely because the interactions were precluded due to lyophobic colloid stabilization through electrostatic repulsion in aqueous media.[28]

The Raman spectra and I-V characteristics supported the presence of noncovalent intermolecular interactions by revealing carrier doping or phonon scattering due to the monovalent ionic adsorbates on the $\pi$ system, as shown in **Figure 4**. Charge transfer occurred from the sodium cations, which acted as donors to the RGO and, hence, the Fermi level of graphene was shifted up to the conduction band.[29,30] The sodium ions in the aqueous NaOH acted as a dopant on RGO, as revealed in the reduction potential measurements. The reduction potentials (versus a standard hydrogen electrode) of $Na^+$ and graphene were –2.71 and +0.14 V, respectively.[31,32] Negative relative reduction potentials from graphene to $Na^+$ indicated that $Na^+$ spontaneously donated electrons to the graphene.

The reduction potential is exclusively correlated with the electron transfer mechanism between graphene and dopant. The material with higher reduction potential can have a greater tendency to accept electrons from that with lower reduction potential. For instance, because $Au^{3+}$ ion has higher reduction potential (+1.50 V) compared to the graphene (+0.14 V) electron transfer from graphene to $Au^{3+}$ can be spontaneously occurred, such that the graphene shows a *p*-type behavior. In the case of $Na^+$ ion, whereas, electron transfer from $Na^+$ ion to graphene is not favorable in spite of the $Na^+$ (–2.71 V) ion has lower reduction potential than graphene. In order to transfer electron from $Na^+$ valence state to graphene spontaneously, $Na^+$ should be preferentially reduced to $Na^0$ state. Columbically interacted $Na^+$ ion to graphene in our work may be reduced by hydrazine, and transformed to $Na^0$ state. Simultaneously, the $Na^0$ becomes stabilized by donating electrons to graphene and is thus transformed again into $Na^+$ which means the cation–$\pi$ interaction is still valid. Therefore, the dispersion stability of CIGO retained during the hydrazine reduction process. As a good agreement, the potassium has been introduced one of n-type dopant for graphene and CNT. Consequently, the cation-pi interaction retained after hydrazine reduction which confirmed by dispersion stability on the CIRGO. As a previous report, ammonia was used for colloidal suspension of rGO.[16] After hydrazine reduction, the rGO without ammonia was agglomerated against ammonia used one. Although the $NH_3^+$ ion incorporated with graphene, the surface of rGO revealed negative charge. The zeta potential confirmed that the rGO solution with ammonia presented negative value. Subsequent hydrazine reduction of CIGO, the Fermi level of graphene was shifted up within the conduction band due to the donation of electrons near the Dirac point. Figure 4a revealed the Raman spectra for RGO and CIRGO. Second-order zone boundary phonon (2D) peaks were observed at 2658 and 2662 $cm^{-1}$ with a symmetric line shape, confirming the presence of single-layered graphene. The intensity ratios of the 2D and G ($I_{2D}/I_G$) bands were 0.51 and 0.37, respectively. In the CIRGO, the $I_{2D}/I_G$ ratio was reduced by cation adsorption due to the introduction of ionic scattering.[33]

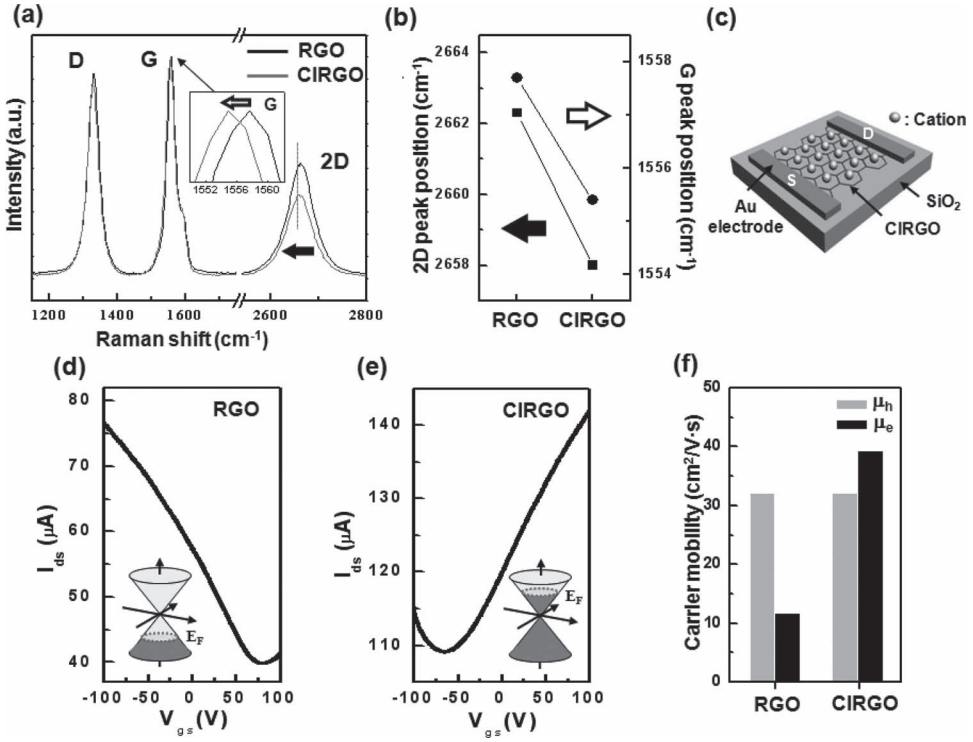


**Figure 4.** Electrostatic stabilization of cation–π interactions, verified from the n-type doping effects of the CIRGO. a) Raman spectra with respect to the non-interacting RGO and CIRGO (inset: the gray arrow reveals the down-shift of the G band). The down-shift and decreased intensity of the 2D band confirmed the presence of n-type doping effects. b) The 2D and G peak positions revealed a down-shift compared to the RGO and CIRGO. c) Schematic diagram showing the fabrication of CIRGO-FET with 300 nm thick on a $SiO_2$ substrate. (d), (e) $I_{ds}$-$V_{gs}$ characteristics of the non-interacting RGO and CIRGO in the gate bias range from −100 ~ 100 V at a constant $V_{ds}$ (0.2 V). d) The non-interacting RGO revealed a Dirac point at a positive gate bias (inset: the band diagram showing the Fermi level ($E_F$) below the valence band). e) The CIRGO displayed *n*-type characteristics (inset: the $E_F$ is located above the Dirac point and is closed to the conduction band). f) Comparison of the carrier mobilities for the RGO and CIRGO ($\mu_h$: hole and, $\mu_e$: electron mobility).

Furthermore, the position of the 2D peak corresponding to doped RGO was shifted with respect to the corresponding peaks of CIRGO and RGO, which could be described by the introduction of electron-phonon coupling which tuned by charge doping effect.[34] Generally, the phonon frequency of the 2D peak can be decreased by electron-phonon coupling which is described by phonon softning. The charge transfer from the sodium ions to graphene significantly downshifted the 2D peak from RGO to CIRGO, as shown in Figure 4b. The usual peak shift due to doping effect was observed on the G band, in good agreement with previous reports.[35,36] These results demonstrated the presence of *n*-type doping effect and phonon scattering due to charge transfer and ionic adsorption, which introduced electrostatic interactions between cations and the aromatic π system. The doping effect was characterized by fabricating an RGO-field effect transistor (FET), as shown in Figure 4c. The electrical properties of the single layered RGO were measured for deposited Au source and drain electrode widths of 2 μm. The $I_{ds}$-$V_{gs}$ curves were observed over a gate voltage range of–100 to 100 V with a constant $V_{ds}$ of 0.2 V. Figures 4d and 4e show that the RGO-FET typically yielded ambipolar characteristics under vacuum conditions at $10^{-3}$ torr due to a decrease in the environmental adsorbates. Figure 4d shows typical *p*-type characteristics for the RGO due to the presence of oxygen moieties, in good agreement with the XPS analysis. The Fermi level of RGO was present in the valence band, as shown in the inset of Figure 4d. Despite the similar atomic percentage of oxygen functional groups with RGO, the Dirac point of CIRGO was shifted to the negative gate bias region indicating the *n*-type doping effect in terms of cation adsorption on the π system as shown in Figure 4e. The effective mobility was calculated from the linear region of the $I_{ds}$-$V_{gs}$ curves using the equation:

$$\mu = Lg_m / WC_0V_{ds,}$$

where $\mu_h$ is the hole mobility, $\mu_e$ is the electron mobility, W and L are the channel width and length, $g_m$ ($dI_{ds}/dV_{gs}$) is the transconductance, $C_0$ is the capacitance for 300 nm thick silicon oxide, and $V_{ds}$ is the drain–source voltage.[37,38] Figure 4f shows that $\mu_h$ for the RGO and CIRGO were similar, 31 $cm^2$/Vs, with the same degree of functional group deoxygenation, which agreed well with the XPS analysis shown in Figure 3d and 3e. In contrast, $\mu_e$ for the CIRGO (39 $cm^2$/Vs) was significantly higher than that of the non-interacting RGO (11 $cm^2$/Vs) due to *n*-type doping effect from the electrostatic interactions between a monopole (cation) and a quadrupole (aromatic π system), as detected in the strong correlations of the $^{13}C$ NMR and Raman spectra. The carrier mobility of CIRGO revealed higher on the order of magnitude compared to the previous work which introduced negatively charged tetrasodium 1,3,6,8-pyrenetetrasulfonic acid (TPA) molecules.[39] The stable dispersion of

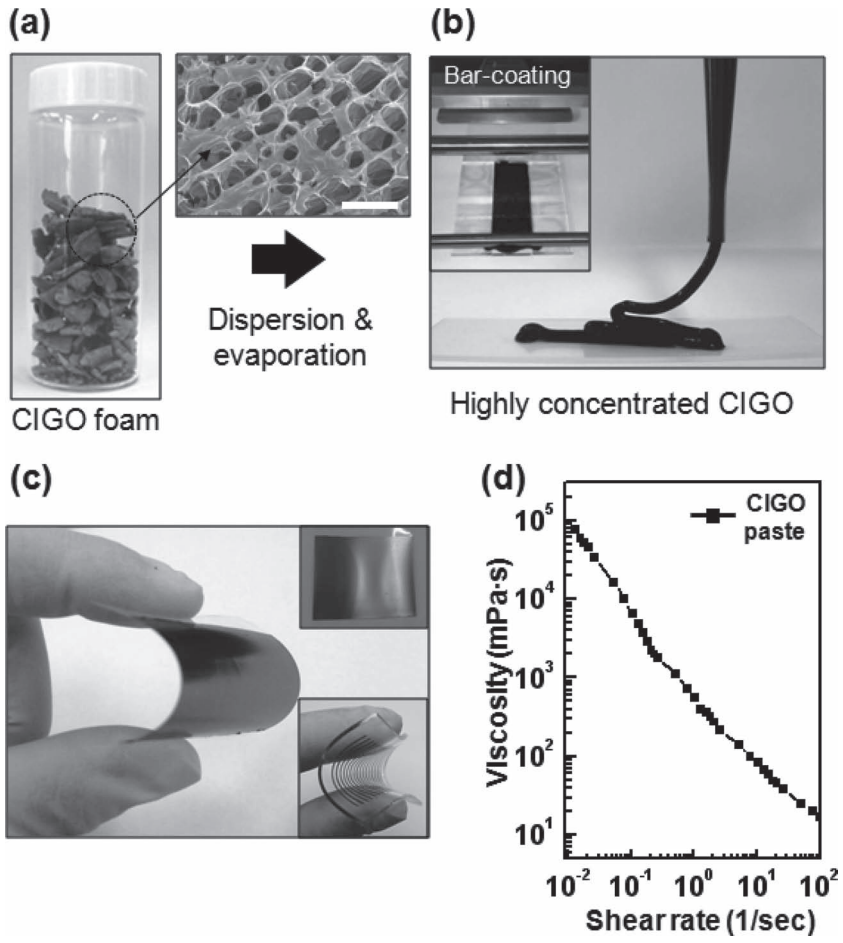


**Figure 5.** Mass production of highly concentrated CIGO and its application to printed electronics. a) Production of foam-like CIGO structures after a freeze-drying process (black arrow: SEM image of the CIGO, the scale bar indicates 100 μm). b) highly concentrated CIGO paste, prepared by additional condensation processes, to yield a high viscosity (inset: CIGO film formation using bar-coating method). c) Bar-coated CIRGO on a PET substrate (inset: uniform coating on PET and a patterned CIRGO on PDMS substrate). d) Viscosity measurements of the highly concentrated CIGO paste.

CIGO and CIRGO permitted formation of a uniform film by filtration. Figure S1 shows the SEM image of the surface and cross-section of CIRGO film which revealed the excellent electrical conductivity without heat treatment, 97,500 S/m. This conductivity was three times higher than that described previously.[40] The non-interacting RGO could not be used to fabricate films due to agglomeration in the aqueous solution. These results demonstrated that the dispersion of highly concentrated RGO was sensitive to the presence of monovalent cation–$\pi$ interactions.

Mass production of an easily-dispersible CIGO powder was achieved by improving the effective interactions of alkali ions with a $\pi$ system. The cation–$\pi$ interactions were accelerated by boiling a GO dispersion in KOH at 100 °C for 2 h, which increased the number of $sp^2$ carbons upon mild deoxygenation. Subsequently, the CIGO solution was concentrated by rotary evaporation to a 50 vol% starting solution, then centrifuged at 10,000 rpm for 1 h three times to remove residual alkali metal ions. The concentration of the final sediment was as high as 20 g/L and the dispersion was highly viscous. Finally, the CIGO powder was obtained by freeze-drying the CIGO slurry. As shown in **Figure 5**a, the CIGO revealed a foam-like structure after removal of ice during the freeze-drying process. The structure could be redispersed in DMF or water with simple sonication. By control of evaporation of solvent, a high-concentration black-colored CIGO paste was obtained with high viscosity, as shown in Figure 5b. A uniform CIRGO film coating on plastic substrates such as PET and PDMS was prepared by the bar-coating method after fuming reduction by hydrazine at 100 °C, as shown in Figure 5c. The electrical resistivity of CIRGO film is ~$10^{-3}$ Ωcm which is lower than that of the conducting films using conventional carbon black (~$10^{-1}$ Ωcm) as well as CNT paste (~$10^{-1}$ Ωcm). The resistivity of the thin film was measured using four-point probe by a van der pauw method. Significantly, the rheological properties of the CIGO paste were verified by viscosity measurements, as shown in Figure 5d. The viscosity provided a physical indication of the quality and dispersibility of the paste. The CIGO paste revealed a high viscosity of $10^5$ mPas at a $10^{-2}$ $sec^{-1}$ shear rate under ambient conditions, which is comparable to the viscosity of conventional silver paste.[41] In contrast, condensation of the non-interacting GO was prevented by aggregation, as showed in Figure 3d. These results demonstrate that monovalent cation–$\pi$ interactions are crucial for stabilizing a dispersion of highly concentrated GO and RGO with high quality. Conducting pastes exist numerously such as graphite, carbon, metal, and CNT-based pastes. Substantially, the metal based conducting paste such as silver shows high conductivity. However, application of the conducting paste has limited in printed electronics. For instance, carbon based thin film transistor and organic photovoltaic need to compatible work function at the interface between conducting electrode (source and drain) and active channel. Therefore, carbon based materials such as CNT and graphene have been introduced. In the case of CIGO paste, it can be used directly to prepare printed electronics by screen printing, bar-coating, or roll-to-roll processes.

## 3. Conclusions

We produced a highly concentrated and conductive RGO containing a low number of oxygen functional groups on the GO. Noncovalent binding interactions between monovalent cations (monopole) such as $Na^+$ or $K^+$, and $sp^2$ carbons (quadrupole) on graphene were obtained by simple aging process with adding an alkaline solution to the aqueous GO solution. In addition,

the RGO dispersion stability was sensitive to the GO solution aging time after the exfoliation process, regardless of the solvent. A highly concentrated CIGO dispersion could be obtained in a concentration as high as 20 g/L. The CIRGO film prepared without post-annealing processes revealed an excellent electrical conductivity of 97,500 S/m at a thickness of 1.7 μm. The proposed approach is straightforward and enables the practical implementation of printed electronics manufacturing to prepare thin film transistors, flexible conducting electrodes, and electrodes for energy devices.

## 4. Experimental Section

*Preparation of RGO nanosheets by monovalent cation–π interaction*: Graphite oxide was synthesized using a modified Brodie method.[10] Pure graphite (Alfa Aesar, 99.999% purity,–200 mesh) was mixed with fuming nitric acid and sodium chlorate at room temperature with stirring for 48 h. After acid treatment, the product was purified by washing, filtering, and cleaning. The synthesized graphite oxide was immersed in aqueous NaOH or KOH at pH 10 to a concentration of 300 mg/L, and exfoliation and dispersion were carried out by sonicating for 1 h. Subsequently, the aging process was perfomed from 0 min to 1400 min respectively as shown in Figure 2a. Aqueous hydrazine monohydrate ($N_2H_4$, 4 mM) was added dropwise to the GO solutions, followed by heating at 100 °C for 16 h. To confirm the dispersion stability of RGO in various solvents with respect to cation-π interacting and non-interacting GO, the GO solution were diluted in dimethylsulfoxide (DMSO), dimethylformamide (DMF), and DI water to a concentration of 90 wt%, followed by hydrazine reduction.

*Characterization for cation-π interacting RGO with high electrical conductivity*: The absorbance properties as a function of aging time of GO were measured by absorption spectroscopy (using a Varioan Cary winRV). The morphologies and element analysis of GO and RGO were measured by atomic force microscopy (AFM, Park Systems XE-100 Multimodes), and field emission scanning electron microscopy (FE-SEM, HITACHI S4800) with energy dispersive X-ray spectroscopy (EDS). The changes in the carbon to oxygen atomic ratio in the functional groups of the RGO were identified by the X-ray photoelectron spectroscopy (XPS) using a Multilab 2000 (Thermo VG Scientific Inc.) spectrometer with monochromatized Al Kα X-ray radiation as the X-ray excitation source. The power was set to 150 W and the voltage to 20 eV for high-resolution scanning, and a 500 μm diameter beam size was used. The fitted peaks of XPS spectra were determined by considering a combination of Gaussian and Lorentzian distribution. To identify the cation-p interaction, high-resolution solid state $^{13}C$ NMR (DSX 400MHz) measurement was performed with magic-angle spinning at room temperature. The structural characteristics of the RGO sheets were investigated by a high-resolution Raman spectrometer (LabRAM HR 800 UV) with an excitation wavelength of 633 nm (1.96 eV) and a Rayleigh line injection filter with a spectral range of 100-3600 $cm^{-1}$ to account for the Stokes shift. To confirm the electrical properties of single layered RGO, the $I_{ds}$-$V_{gs}$ measurement was performed by two-probe measurement (Keithley 4200-SCS) to characterize the carrier mobility and type of the CIRGO and non-interacting RGO at vacuum condition of $10^{-3}$ torr. The supernatant RGO solution was dropped onto a 300 nm thick $SiO_2$ substrate. The electrode pattern was obtained using conventional photolithography process. The channel width and length of metal electrode was 2 and 6 μm. The Cr and Au electrodes were deposited using a thermal evaporator with a thickness of 20 and 100 nm, respectively. Also, the CIRGO film was prepared by filtration and then dried at 80 °C in ambient condition. The electrical conductivity was measured by four-point probe method (Keithley 2000 multimeter) at room temperature.

*Mass production of cation-π interacting GO and paste formation:* The cation–π interacting GO (CIGO) powder and slurry were prepared by stepwise evaporation and centrifugation. The cation–π interactions were accelerated by boiling a GO dispersion in NaOH or KOH at 100 °C for 2 h. Subsequently, the CIGO solution was concentrated by rotary evaporation to a 50 vol% starting solution, and then centrifuged at 10,000 rpm for 1 h three times. The concentration of final sediment was as high as 20 g/L and the dispersion was highly viscous. The CIGO paste was uniformly coated on polydimethylsiloxane (PMDS) substrate by bar-coating method (Barcoater: Elcometer automatic film applicator 4340). The viscosity of CIGO paste was measured by rheometer (Brookfield DV-III ultra).

## Supporting Information

Supporting Information is available from the Wiley Online Library or from the author.

## Acknowledgements

This work was supported by a grant from the Fundamental R&D Program for Core Technology of Materials funded by the Ministry of Knowledge Economy, and by a grant (Code No. 2011-0032157) from the Center for Advanced Soft Electronics under the Global Frontier Research Program of the Ministry of Education, Science and Technology, Korea.

Received: January 26, 2012
Revised: March 2, 2012
Published online: April 30, 2012

[1] K. S. Novoselov, A. K. Geim, S. V. Morozov, D. Jiang, M. I. Katsnelson, I. V. Grigorieva, S. V. Dubonos, A. A. Firsov, *Nature* **2005**, *438*, 197.
[2] C. Lee, X. Wei, J. W. Kysar, J. Hone, *Science* **2008**, *321*, 385.
[3] A. A. Balandin, S. Ghosh, W. Bao, I. Calizo, D. Teweldebrhan, F. Mial, C. N. Lau, *Nano Lett.* **2008**, *8*, 902.
[4] K. I. Bolotin, K. J. Sikes, Z. Jiang, M. Klima, G. Fudenberg, J. Hone, P. Kim, H. L. Stormer, *Solid State Commun.* **2008**, *146*, 351.
[5] K. S. Novoselov, A. K. Geim, S. V. Morozov, D. Jiang, Y. Zhang, S. V. Dubonos, I. V. Grigorieva, A. A. Firsov, *Science* **2004**, *306*, 666.
[6] C. Berger, Z. M. Song, X. B. Li, X. S. Wu, N. Brown, C. Naud, D. Mayou, T. B. Li, J. Hass, A. N. Marchenkov, E. H. Conrad, P. N. First, W. A. de Heer, *Science* **2006**, *312*, 1191.
[7] K. S. Kim, Y. Zhao, H. Jang, S. Y. Lee, J. M. Kim, K. S. Kim, J. Ahn, P. Kim, J. Choi, B. H. Hong, *Nature* **2009**, *457*, 706.
[8] S. Stankovich, D. A. Dikin, G. H. B. Dommett, K. M. Kohlhaas, E. J. Zimney, E. A. Stach, R. D. Piner, S. T. Nguyen, R. S. Ruoff, *Nature* **2006**, *442*, 282.
[9] S. Park, R. S. Ruoff, *Nat. Nanotechnol.* **2009**, *4*, 217.
[10] B. C. Brodie, *Philos. Trans. R. Soc. London* **1859**, *149*, 249.
[11] W. S. Hummers, R. E. Offeman, *J. Am. Chem. Soc.* **1958**, *80*, 1339.
[12] H. P. Boehm, W. Scholz, *Justus Liebigs Ann. Chem.* **1965**, *691*, 1.
[13] H. Jeong, Y. P. Lee, R. J. W. E. Lahaye, M. Park, K. H. An, I. J. Kim, C. Yang, C. Y. Park, R. S. Ruoff, Y. H. Lee, *J. Am. Chem. Soc.* **2008**, *130*, 1362.
[14] W. Gao, L. B. Alemany, L. Ci, P. M. Ajayan, *Nat. Chem.* **2009**, *1*, 403.
[15] S. Stankovich, R. Piner, X. Chen, N. Wu, S. T. Nguyen, R. S. Ruoff, *J. Mater. Chem.* **2006**, *16*, 155.
[16] D. Li, M. B. Muller, S. Gilje, R. B. Kaner, G. G. Wallace, *Nat. Nanotechnol.* **2008**, *3*, 101.
[17] S. Park, J. An, R. D. Piner, I. Jung, D. Yang, A. Velamakanni, S. T. Nguyen, R. S. Ruoff, *Chem. Mater.* **2008**, *20*, 6592.
[18] S. Park, J. An, I. Jung, R. D. Piner, S. J. An, X. Li, A. Velamakanni, R. S. Ruoff, *Nano Lett.* **2009**, *9*, 1593.
[19] D. A. Dougherty, *Science* **1996**, *271*, 163.
[20] J. Sunner, K. Nishizawa, P. Kebarle, *J. Phys. Chem.* **1981**, *85*, 1814.

[21] E. Choi, T. H. Han, J. Hong, J. E. Kim, S. H. Lee, H. W. Kim, S. O. Kim, *J. Mater. Chem.* **2010**, *20*, 1907.
[22] W. Cai, R. D. Piner, F. J. Stardermann, S. Park, M. A. Shaibat, Y. Ishii, D. Yang, A. Velamakanni, S. J. An, M. Stoller, J. An, D. Chen, R. S. Ruoff, *Science* **2008**, *321*, 1815.
[23] J. Cheng, W. Zhu, Y. Tang, Y. Xu, Z. Li, K. Chen, H. Jiang, *Chem. Phys. Lett.* **2002**, *366*, 267.
[24] L. B. Casabianca, A. C. de Dios, *J. Chem. Phys.* **2008**, *128*, 052201.
[25] C. Bravo-Diaz, M. Soengas-Fernandez, M. J. Rodriguez-Sarabia, E. Gonzalez-Romero, *Langmuir* **1998**, *14*, 5098.
[26] C. Mattevi, G. Eda, S. Agnoli, S. Miller, K. A. Mkhoyan, O. Celik, D. Mastrogiovanni, G. Granozzi, E. Garfunkel, M. Chhowalla, *Adv. Funct. Mater.* **2009**, *19*, 1.
[27] X. Fan, W. Peng, Y. Li, X. Li, S. Wang, G. Zhang, F. Zhang, *Adv. Mater.* **2008**, *20*, 4490.
[28] D. H. Everett, *R. Soc. Chem., London* **1988**, 243.
[29] B. Sachs, T. O. Wehling, A. I. Lichtenstein, M. I. Katsnelson, *Physics and Applications of Graphene, InTech* **2011**, 30.
[30] H. Shin, W. Choi, D. Choi, G. H. Han, S. Yoon, H. Park, S. Kim, Y. W. Jin, S. Y. Lee, J. M. Kim, J. Choi, Y. H. Lee, *J. Am. Chem. Soc.* **2010**, *132*, 15603.
[31] B. Kong, J. Geng, H. Jung, *Chem. Commun.* **2009**, 2174.
[32] H. Reiss, A. Heller, *J. Phys. Chem.* **1985**, *89*, 4207.
[33] A. Das, S. Pisana, B. Chakraborty, S. Piscanec, S. K. Saha, U. V. Waghmare, K. S. Novoselov, H. R. Krishnamurthy, A. K. Geim, A. C. Ferrari, A. K. Sood, *Nat. Nanotechnol.* **2008**, *3*, 210.
[34] Y. Zhu, S. Murali, W. Cai, X. Li, J. W. Suk, J. R. Potts, R. S. Ruoff, *Adv. Mater.* **2010**, *22*, 3906.
[35] D. Choudhury, B. Das, D. D. Sarma, C. N. R. Rao, *Chem. Phys, Lett.* **2010**, *497*, 66.
[36] X. Dong, D. Fu, W. Fang, Y. Shi, P. Chen, L. Li, *Small* **2009**, *5*, 1422.
[37] S. Y. Jeong, S. H. Kim, J. T. Han, H. J. Jeong, S. Yang, G. Lee, *ACS Nano* **2011**, *5*, 870.
[38] C. Su, Y. Xu, W. Zhang, J. Zhao, X. Tang, C. Tsai, L. Li, *Chem. Mater.* **2009**, *21*, 5647.
[39] X. Dong, C. Su, W. Zhang, J. Zhao, Q. Ling, W. Huang, P. Chen, L. Li, *Phys. Chem. Chem. Phys.* **2010**, *12*, 2164.
[40] I. K. Moon, J. Lee, R. S. Ruoff, H. Lee, *Nat. Commun.* **2010**, *1*, 73.
[41] S. P. Wu, L. Q. Zheng, Q. Y. Zhao, X. H. Ding, *Colloids Surfaces A: Physicochem. Eng. Aspects* **2010**, *372*, 120.